Microfluidic platform for screening the activity of immobilized photocatalysts for degradation of organic water pollutants

Anca Roibu[a]*, Razvan Udroiu[b], Alexandru Dinu[c], Luminita Andronic[a]*

[a] Product Design, Mechatronics and Environment Department, Transilvania University of Brasov, Romania
[b] Manufacturing Engineering Department, Transilvania University of Brasov, Romania
[c] Electronics and Computers Department, Transilvania University of Brasov, Romania

*Corresponding authors: Anca Roibu (e-mail: anca.roibu@unitbv.ro), Luminita Andronic (e-mail: andronic-luminita@unitbv.ro)

Abstract

Photochemistry screening platforms have the potential to accelerate the discovery and development of new photocatalysts. This study presents the design and characterization of a novel activity screening platform of immobilized photocatalytic films for degrading water pollutants. The compact testing system is engineered with four 3D-printed microreactors and a rotative multi-wavelength LED light source, which is capable of emitting at the 395, 409, 413, and 443 nm. Despite the different LEDs being placed in a compact space, 95% of the light that reaches the photocatalytic films is emitted by the LEDs directly opposite them. Therefore, the design allows for a minimum of 16 distinct testing conditions by simply rotating the light source. The performance of the microfluidic platform was characterized using the photocatalytic degradation of a pesticide, imidacloprid, in the presence of P25 TiO_2, immobilized as thin film on glass plates. The results demonstrated a consistent degradation efficiency of around 35 % at 395 nm, with negligible variation across the four microreactors and no influence of the testing order at 395, 409, 413 and 443 nm. Notably, the photocatalytic film activity did not decrease after 6 hours of operation and under five successive illumination conditions. The screening conditions were optimized using the dynamic water infusion which increased the degradation efficiency of the imidacloprid to 71 %. In addition, the dynamic illumination allowed the sequential operation of the 4 types of LEDs, and led to a halved degradation efficiency despite the LEDs were lighted up for only a quarter of the time. This microfluidic platform diminishes the manual labor and the quantities of photocatalyst and polluted water required per test compared to the batch screening, consequently, it emerging as an efficient and sustainable tool that is suitable for the automated screening of immobilized photocatalysts.

1 Introduction

Screening platforms are promising tools for accelerating the discovery and development of new light-driven transformations and photocatalysts characterized by improved efficiency. In recent years, the screening of photochemical reactions in flow has experienced impressive progress, with advances in reagent solutions preparation and handling, photoreactor design, analysis, automated operation, and optimization algorithms.[1–16] Eyke et al. reported an automated multiphase platform equipped with 10 parallel reactor channels out of which a channel was adapted to screen photochemical reactions by integrating an LED board[3]. Moreover, a robotic platform with a capillary reactor irradiated by 6 LED modules was reported by Slattery et al.[4] Considerably fewer studies described screening platforms in which heterogeneous photocatalysts are involved as slurry[10], imprinted polymer nanoparticles[17] and immobilized on glass beads[18].

While the reported testing systems were predominantly applied for discovery and optimization in organic synthesis, the research efforts focused on developing photocatalysts for degrading water pollutants could benefit from using screening platforms. The high-throughput testing of heterogeneous photocatalysts for degrading contaminants such as methyl orange, methylene blue, Congo red, Rhodamine B, 4-chlorophenol, terephthalic acid, the steroid 17α-ethinylestradiol, histamine, progesterone, and caffeine has been mostly performed in batch photoreactors.[19–25] However, screening in microreactors proved to be not just fast and reproducible [26], but also reduced the reagent and photocatalyst consumption [27]. Using solid photocatalysts in flow is challenging, and various solutions were described like immobilization as a thin film, [26,28–30] loading particles as dry powders into microchannels [27] and 3D printing using a mixture of the photocatalyst with a polymeric material[31].

The wavelength-dependent activity of the prepared photocatalysts is important, especially in the case of materials for which the absorbing properties were extended towards visible and near-infrared domains to improve the utilization of solar radiation.[32] Roider et al. reported a flow photoreactor equipped with an automated change of the irradiation wavelength showing that small differences between the incident wavelength can significantly affect the product formation.[14] Previously, we validated a methodology in which the activity of reduced TiO_2 photocatalysts for degradation of a pesticide, imidacloprid (IMD), was investigated using a single immobilized photocatalytic film placed in a microreactor successively irradiated at 395, 413, and 443 nm using a rotative LED light source.[33] In this study, we present the integration of the developed methodology into a microfluidic platform with 4 parallel 3D printed microreactors and a multi-wavelength LED light source. The microfluidic platform was characterized from the point of view of photon irradiance and reproducibility of the IMD degradation in the 4 microreactors. Next, the influence of the screening order at 395, 409, 413, and 443 nm on the IMD degradation by TiO_2 P25 is investigated. Finally, the screening conditions are optimized by implementing dynamic flow and dynamic irradiation to increase the degradation efficiency and enable the simultaneous operation of the microreactors.

Materials and methods

2.1 Design of the AutoMATiO microfluidic screening platform

A compact and modular microfluidic platform was designed to screen immobilized photocatalysts, as shown in Figure 1, that we named AutoMATiO. It consists of an enclosure created by placing four 3D-printed supports on a rectangular metal structure and attaching four 3D-printed

2

microreactors to these supports. A LED light source containing 4 types of LEDs grouped in the function of the emitted wavelength (395, 409, 413, and 443 nm) was placed in the center of the enclosure. The sides of the platform are protected by two 3D-printed covers, one equipped with 4 radial fans and the other with openings for air circulation. The LED light source is rotated using a stepper motor to select the irradiating wavelength for a certain microreactor. The microreactors are removable from the supports and are equipped with an exchangeable glass plate on which the investigated photocatalyst is deposited.
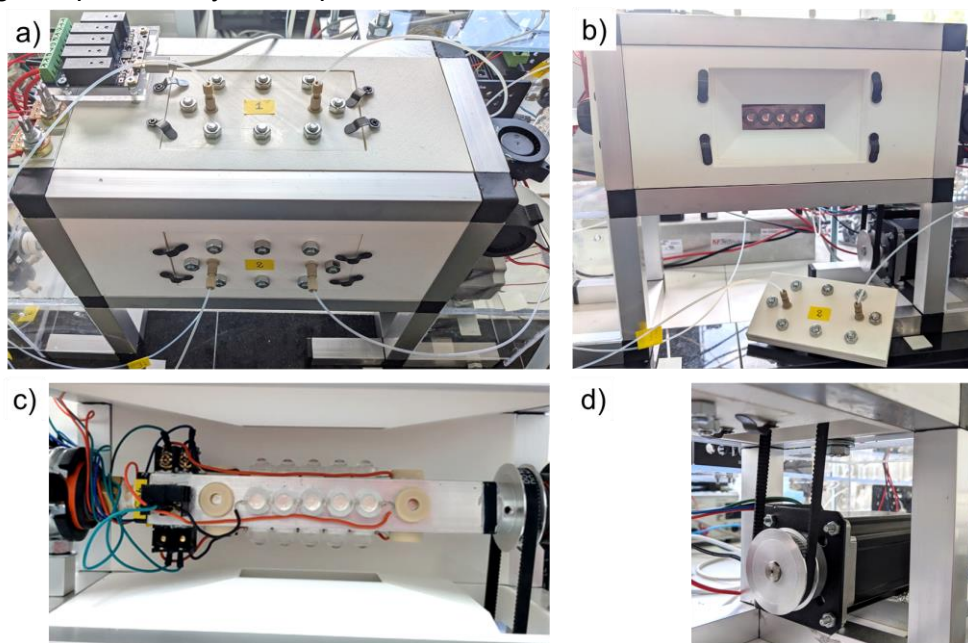

Figure 1 Image representation of AutoMATiO microfluidic screening platform.

2.2 3D printing of microreactors and supports

The microreactor components were designed using the SolidWorks 2016 (Dassault Systèmes). Each microreactor consists of component A which contains a channel and component B with the photoreactor window. Their design is illustrated in Figure 2 and was described in our previous work.[33] The reactor channel has a length of 6.7 cm and a squared cross-section of 1 mm. The reactor window defines the illuminated area and is characterized by a length of 6.5 cm and a width of 1.5 cm. [33] The channel was reversibly sealed by the glass plate using a thin silicone layer which was sprayed around the channel and was covered when solidified by a small quantity of silicon grease. In addition, two ports (NanoPort Kit, Upchurch Scientific) were glued on component A to obtain the inlet and outlet connections of the microreactor.
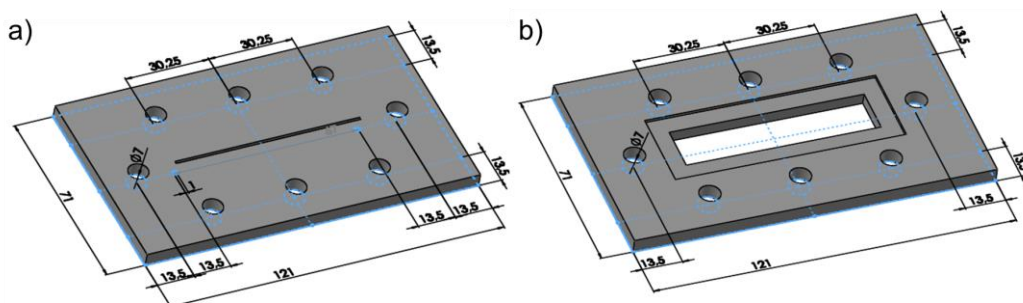

Figure 2 The 3D models of a) component A, and b) component B of the microreactor.
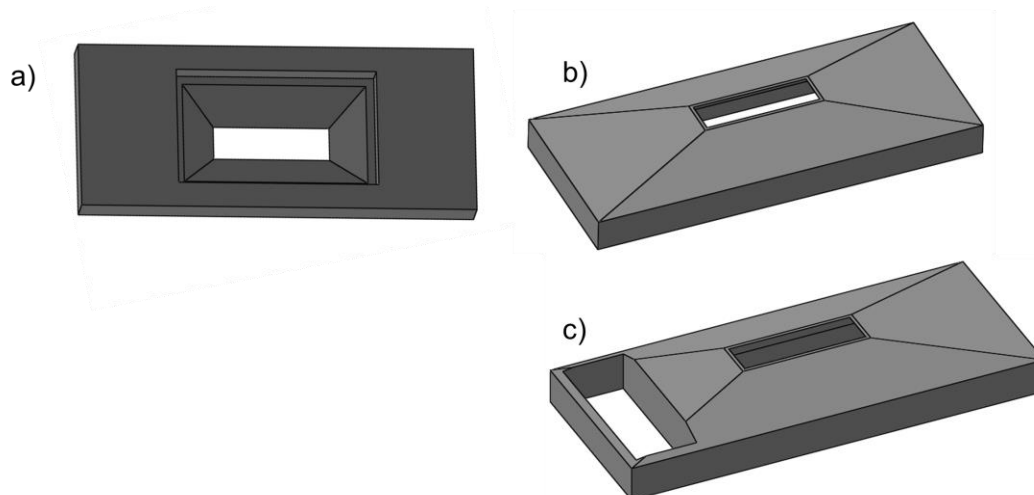
3

Figure 3 The 3D models of the microreactor supports a) front view and b) back view of the support for the microreactors M1, M2, and M4, and c) back view for the support for the microreactor M3.

The 3D models were saved in the stereolithography (STL) file format used as input data in the additive manufacturing process. Fused deposition modeling (FDM) was the 3D printing technique used, which is a technology from the material extrusion category.[34] The 3D printing was performed using a white filament of polylactic acid/ polyhydroxyalkanoate (PLA/PHA) with a filament diameter of 2.85mm. PLA/PHA is a tougher and less brittle material than the generic PLA grades. PLA is a bioplastic and thermoplastic made from natural materials such as corn starch. PHA is a bio-polyester produced by fermentation processes within bacteria and is also 100 % biodegradable. The components were manufactured using the BCN3D Sigma X printer. The preprocessing step was performed using BCN3D Cura version 3.4.1 software. The main 3D printing parameters for the microreactor parts A and B were a hotend of 0.4 mm in diameter, a deposited layer thickness of 0.2 mm, infill density of 40 %, a build plate temperature of 60 °C and the printing temperature of the extruder of 210 °C. The manufacturing time was 5h 25 min for component A and 5h 29 min for component B. Two types of microreactor supports were designed, for the microreactors M1, M2, and M4 as shown in Figures 3a-b, and for the microreactor M3 illustrated in Figure 3c. All the supports are characterized by a window that allows the light coming from the LEDs facing the support to reach the contained microreactor. The supports were designed in-house using SolidWorks 2016 and 3D printed by Next3D Additive Solutions (Romania). In addition, two platform covers were designed using SolidWorks 2016 and 3D printed, the manufacturing time being 5h 56 min.

2.2 Immobilization of the photocatalyst

Powdered TiO_2 (P25/20, VP Aeroperl, Evonik), referred to in this study as P25, was deposited on soda lime glass plates (2.6 × 7.5 × 0.1 cm, Thermal Fisher) by spray coating using a nozzle connected to a compressed air pump. A metal mask was used during spraying to obtain a coated area of 8.7 cm^2. The glass was first heated to 150 °C and then sprayed with a sonicated ethanol suspension of the photocatalyst (7 g/L). Multiple thin layers were applied with a waiting time of 30 s, which were then left to dry for 20 min at the same temperature. As can be observed in Figure 4, a homogeneous film is obtained. Weight and light transmission were used as measures to quantify the amount of deposited TiO_2 on different glass plates. Finally, the glass plate with the immobilized photocatalyst is inserted between components A and B of the microreactor.
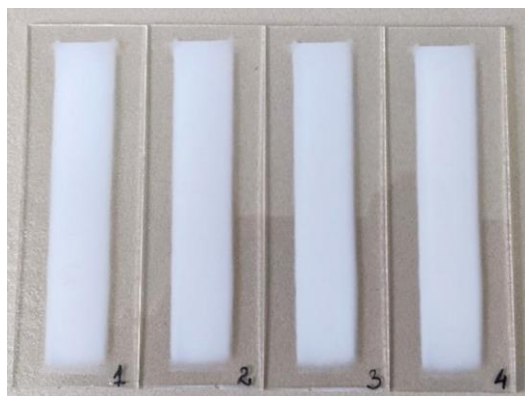
4

Figure 4 Image of the immobilized TiO_2 P25 films tested in the 4 microreactors.

2.3 Light source design and characterization

The light source contains 4 groups of LEDs emitting at the maximum wavelengths λ_{max} of 395, 409, 413, and 443 nm. Each group consists of 5 high-power LEDs (3 W) that are connected in series and are characterized by a viewing angle of 140°. To ensure that the emitted light is directed toward the microreactor, polymeric lenses were used to obtain a viewing angle of 30°. As shown in Figure 5a, the LEDs were immobilized on an aluminium square tube through which water was continuously recirculated by a cooler (CW-3000DG, Vevor). The light source is connected to the coolant tubing by hydraulic quick couplings that permit the rotation of the light source without water leakage. To switch between different light source positions as shown in Figure 5c, the light source was rotated in steps of 90° clockwise and counter-clockwise by a stepper motor (Nema 23, StepperOnline), 2 timing pulleys (i.e. a timing pulley fixed on the light source and a second one located on the stepper motor), and a timing belt. The stepper motor was connected to a digital stepper driver (DM556T, StepperOnline) that was controlled by a microcontroller board (Uno R3, Arduino) and Arduino software, IDE. The LED groups were powered one at a time with a bench power supply (BK1697B, B&K Precision), and the selection was performed using 4 switches integrated on a module (Yocto-MaxiPowerRelay, Yoctopuce) controlled by VirtualHub (Yoctopuce) or a python script.
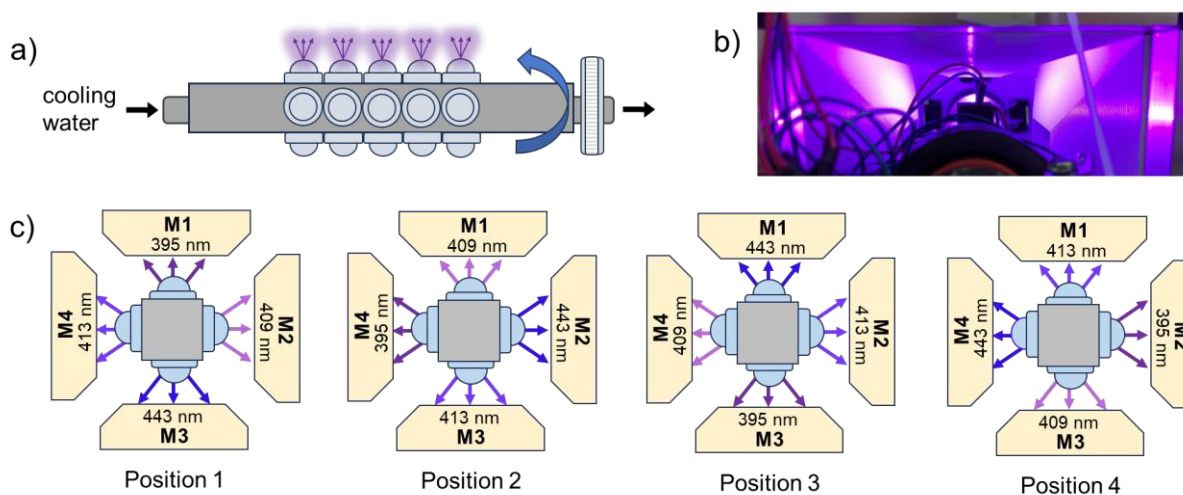

Figure 5 a) Schematic representation of the LED light source, b) image of the light distribution on the microreactor supports, and c) the possible positions of the LED light source.

5

Table 1 Electrical and optical characteristics of the LED light source, measured at the level of the microreactor M1.

LEDs	λ_{max} (nm)	Current (mA)	Voltage (V)	Power (W)	Irradiance (mW cm^{-2})	Photon irradiance·10^3 (Einstein m^{-2} s^{-1})
Group 1	395	330	16.3	5.4	81.8	2.7
Group 2	409	430	17.2	7.4	69.9	2.4
Group 3	443	330	15.4	5.1	72.2	2.7
Group 4	413	430	17.2	7.4	75.6	2.6

As the 4 types of LEDs have different electrical and optical properties, different optical outputs are obtained if the same forward current is used. Therefore, as shown by Table 1, the LEDs emitting at 395 and 443 nm were operated at 330 mA, and the LEDs emitting at 409 and 443 nm at 430 mA, so that relatively similar photon irradiance values are obtained. The irradiance was measured using a cosine corrector (CC-VIS/NIR, Avantes) connected to an optical fiber (UVIR200–2-BX-FC/PC, Avantes) and a calibrated UV-Vis spectrometer (AvaSpec-ULS2048CL-EVO-UA, Avantes). The irradiance was measured behind the glass plate, at the center of the reactor window, and is considered that it indicates the irradiance value on the photocatalytic film. Finally, the LED light source is integrated at the center of the microfluidic platform (see Figure 4c), and additional cooling of the LEDs surface was provided using 4 radial fans placed at one side of the platform.

2.5 Photocatalytic tests in flow

An aqueous solution of IMD with an initial concentration of 2.5 mg L^{-1} was introduced in the flow microreactor using a syringe pump (NE-501 OEM, New Era). The liquid flow rate was controlled from the computer using WinPumpTerm software or by a python script. Before every photocatalytic activity test, the pollutant solution is passed through the photoreactor channel for 30 min so that an adsorption equilibrium is reached, and then two samples of 1 mL were collected, passed through a syringe filter (PES, 0.45 µm), and analyzed by HPLC. Next, the LEDs are turned on, and after waiting for the steady state, 2 samples of 1 mL are collected and similarly processed. The HPLC analysis was carried out using a Shimadzu LC- 20 ADsp instrument equipped with a C18-Macherey Nagel column, Nucleosil 5 µm, and a UV detector SPD-20A set at a wavelength of 270 nm. The mobile phase was acetonitrile: water (70:35, v/v), the flow rate was 1 mL min^{-1}, and the temperature was 40 °C.

For investigating the characteristics of microreactors and light source, the water flow rate was set at 3.5 mL h^{-1}. In addition, for optimizing the conditions for photocatalytic activity screening, three types of experiments were carried out using: (i) dynamic flow and continuous irradiation, (ii) continuous flow and dynamic irradiation, and (iii) dynamic flow and dynamic irradiation. The dynamic flow was implemented to achieve a higher degradation efficiency than in continuous flow by increasing the residence time. Moreover, when the four microreactors are used simultaneously with a single pump connected to a 5-port manifold, we observed an inhomogeneous flow distribution. Applying a dynamic flow that consists of periods of infusing and stop flow is similar to introducing liquid with a pump into one microreactor for a short time, then switching to another microreactor, until the liquid is pumped sequentially into all microreactors. Consequently, if water is pumped through microreactor M1 for 10 s, then after a pathway switch of 1 s, the infusion is performed for 10 s into microreactor M2, and similarly, into M3 and M4, it results in a cycle of Time ON = 10 s and Time OFF = 34 s for each microreactor.

6

Table 2 Characteristics of the continuous and dynamic flow in a microreactor.

Pump flow rate (mL h⁻¹)	Time ON (s)	Time OFF (s)	Average flow rate (mL h⁻¹)	Residence time (min)
3.5	continuous	-	-	1.15
7	5 s	19	1.46	2.76
7	10 s	34	1.59	2.53
7	15 s	49	1.64	2.45
10.5	15 s	49	2.34	1.63

We investigated the degradation efficiency when Time ON is equal to 5, 10, and 15 s, at 7 and 10.5 mL h⁻¹. As shown in Table 2, these conditions lead to larger residence times compared to the reference case at the continuous flow of 3.5 mL h⁻¹ due to the resulting lower average flow rate. Despite different practical implementations, a similar principle was used in stop-flow reactors, that were employed in reaction screening for transformations that were not suitable for screening in conventional flow reactors because of the required long reaction times.[3,35–39] In addition, the oscillating flow was previously used to decouple mixing and residence time in high-throughput parameter screening[40] and to improve the mixing and the residence time distribution in process intensification investigations.[41]

Moreover, a dynamic irradiation approach was considered to allow powering the 4 groups of LEDs with a single power supply. As the LEDs of the light source have different electrical properties, they cannot be easily powered at the same time. Therefore, we used 4 switches to sequentially connect and disconnect each group of LEDs. The obtained dynamic illumination consists of an alternation of light and dark periods as shown in Figure 6. If the irradiating time for each microreactor is equal to Time ON of 0.5 and 1 s, it results in a cycle period of 2 and 4 s, respectively. The values of the duty cycle were calculated using Equation 1, and the values of the average photon irradiance by Equation 2, the results being listed in Table 3.
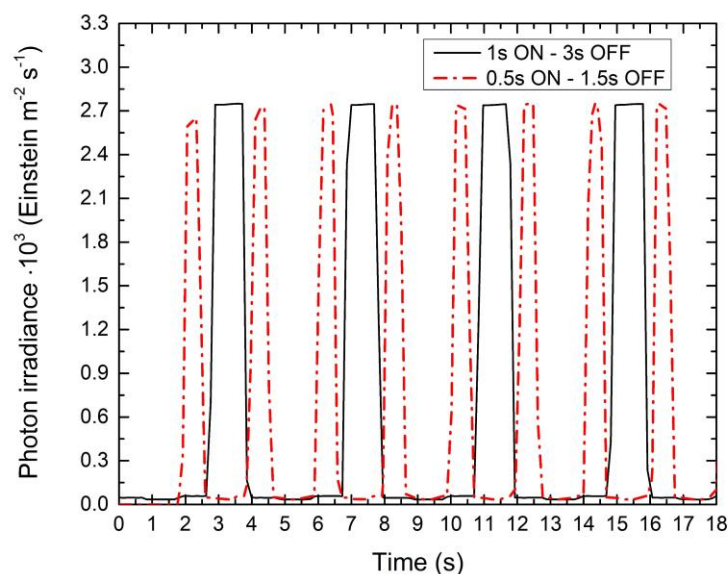

Figure 6 Photon irradiance on the microreactor facing the 395 nm LEDs during dynamic irradiation.

Table 3 The characteristics of the dynamic irradiation at 395 nm.

Time ON (s)	Time OFF (s)	Cycle period (s)	Duty cycle (%)	Average photon irradiance·10^3 (Einstein m^{-2} s^{-1})
0.5	1.5	2	25	0.68
1	3	4	25	0.68

$$\text{Duty cycle} = \frac{\text{Time ON}}{\text{Time ON} + \text{Time OFF}} \times 100 \tag{1}$$

$$\text{Average photon irradiance} = \text{Duty cycle} \times \text{Photon irradiance} \tag{2}$$

The alternation of illumination and dark periods is commonly referred to as controlled periodic illumination (CPI). CPI was previously applied to improve the photonic efficiencies of the photocatalytic degradation of various organic compounds such as methyl orange [42], dimethyl phthalate [43], o-cresol[44] by using the incident light more efficiently.

Finally, the dynamic flow and dynamic irradiation were combined and applied in a photocatalytic test carried out in a microreactor. The implementation of the three types of dynamic conditions was performed using python, the flowcharts of the automation being illustrated in Figure 7.
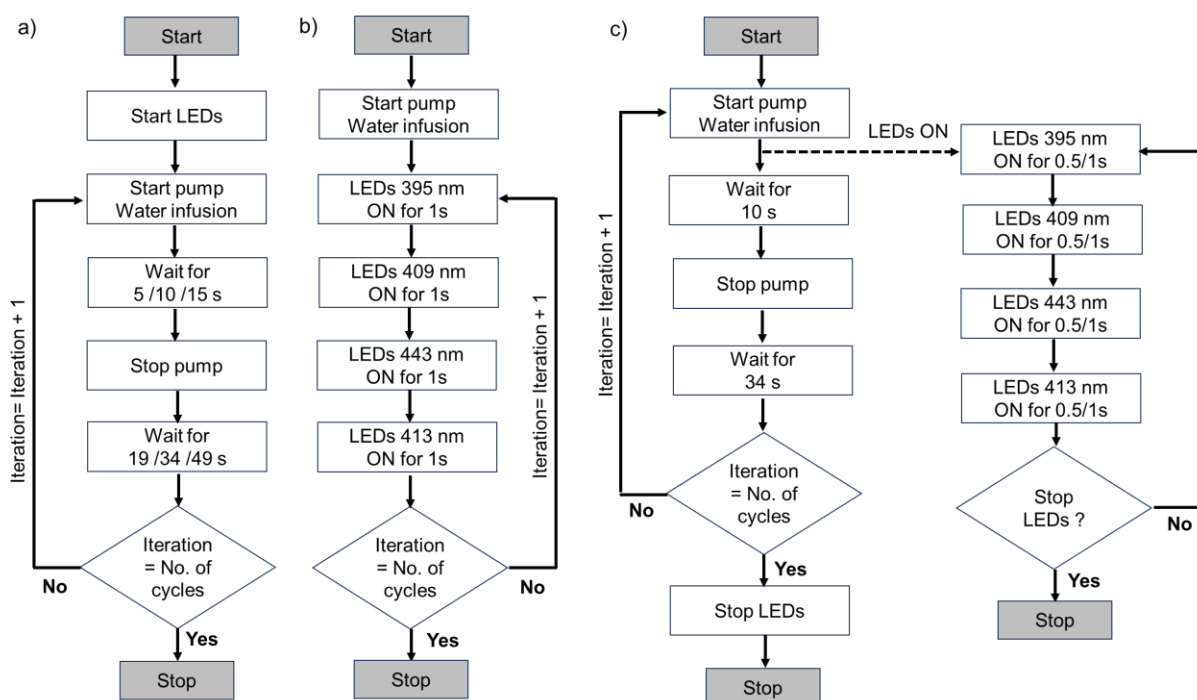

Figure 7 Flowchart for the automation of photocatalytic tests characterized by a) dynamic flow and continuous irradiation, b) dynamic irradiation and continuous flow, and c) dynamic flow and dynamic irradiation.

8

3 Results and discussions

3.1 Characterization of the microfluidic platform

The number of photons reaching the photocatalysts placed in the 4 microreactors is a determining factor in the photocatalytic activity screening. Therefore, photon irradiance was measured at the level of the microreactors M1-M4 that are located on each side of the light source which was set at Position 1. As can be observed from Figure 8, the majority of the light received by a microreactor, at least 95 %, is emitted from the facing LEDs.
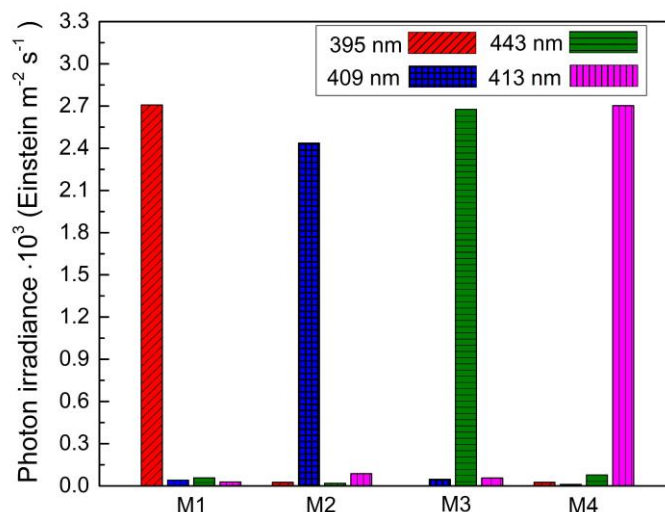

Figure 8 Photon irradiance on microreactors M1, M2, M3 and M4 when the LED light source is set on Position 1.

As the photocatalytic tests are carried out at the desired wavelength (i.e., 395, 409, 413 or 443 nm) with an insignificant influence from the other LEDs, it was demonstrated that the design of the light source and of the 3D-printed supports is efficient. Moreover, there is a maximal standard deviation of 5 %, between the irradiance measured at the level of each microreactor at 395, 409, 413, and 443 nm LEDs. Consequently, the 4 microreactors could be considered similar from the point of view of the incident radiation, irrespective of the LED type.

Moreover, Figure 9 shows that the IMD degradation efficiency in the 4 microreactors containing 4 photocatalytic films is similar at 395 nm.
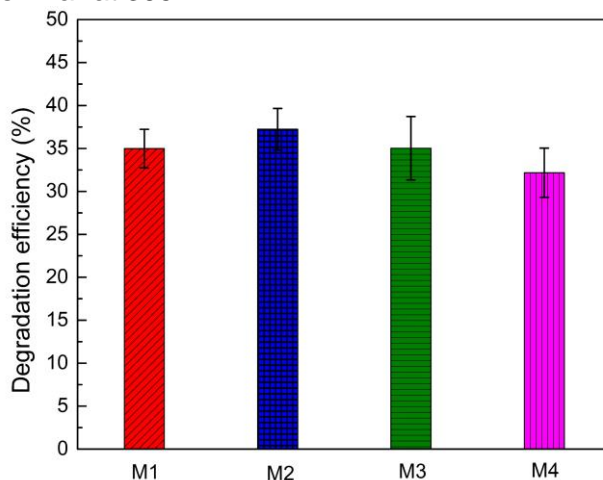

Figure 9 IMD degradation efficiency determined in the microreactors M1, M2, M3, M4 at 395 nm.
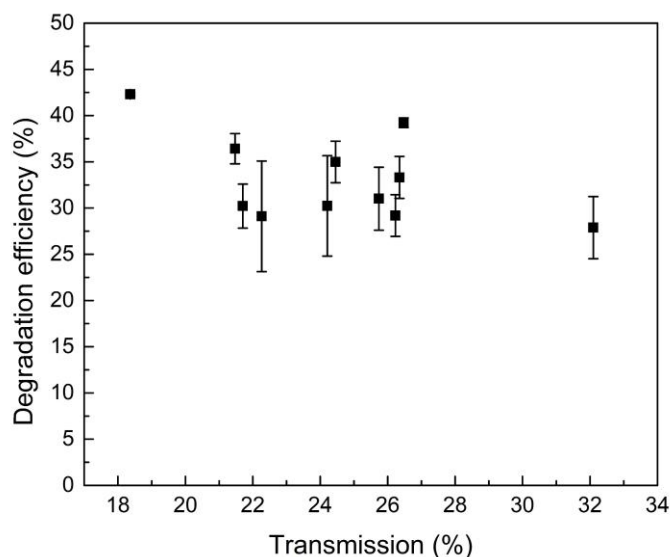
9

Figure 10 IMD degradation efficiency determined in the microreactor M1 at 395 nm in function of 395 nm LED light transmission of the photocatalytic film.

The average degradation efficiency was 34.8 % with a standard deviation of ± 2.1 %, which is below the standard deviation observed for the individual microreactor (2.2-3.7 %), which shows that the microreactors could be considered similar also from the point of view of the reactor channel dimensions, the 3D printing providing a reproducible manufacturing.

Next, the variability caused by the deposition of the photocatalyst on the glass plate and its immobilization between the two microreactor components was investigated. A number of 11 photocatalytic tests were carried out in the microreactor M1 using 11 deposited films of TiO_2 P25. The resulting IMD degradation efficiency is shown in Figure 10 in function of the 395 nm LED light transmission of the tested photocatalytic films. For a light transmission comprised between 18 and 32 %, we observed degradation efficiencies ranging between 42 to 28 %. The degradation efficiency is higher at lower light transmission because of the larger amount of photocatalyst present on the glass plate. Using the transmission measured at 360 nm, we estimate that the film thickness varies between 1.8 and 2.9 μm when the light transmission increases from 18 to 32 %.[33,45,46]

The observed difference between the photocatalytic tests that are performed at similar light transmission, and therefore at the same film thickness, was attributed to the different photocatalytic film surface areas coming into contact with the aqueous solution of IMD. As the boundary, that resulted by pressing the two reactor components together with the solid silicon layer and silicon grease, varied between different measurements, it led to either smaller or higher photocatalyst/ IMD concentration ratios. While this variation came as a price for the straightforward exchangeability of the photocatalytic film, a reproducible surface area of the immobilized photocatalyst which is in contact with the liquid flowing through the channel could be achieved by introducing new elements in the reactor design. Nevertheless, taking into account the degree of standard deviation for each experiment, that is most probably influenced by how fast the equilibrium state is established for each photocatalytic film, it can be concluded that the microreactor is able to offer dependable information about the activity of tested photocatalysts.
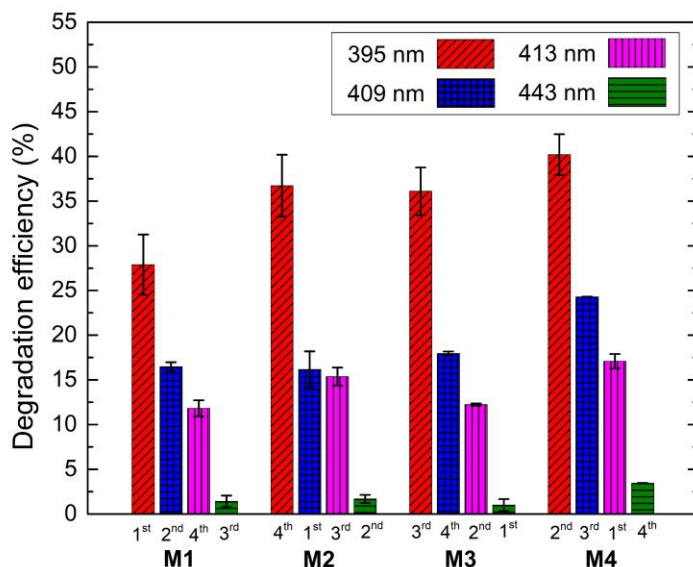
10

Figure 11 IMD degradation efficiency determined in microreactors M1, M2, M3 and M4 at 395 nm, 409, 413, and 443 nm.

If the 4 microreactors are simultaneously employed, they are irradiated in a different order by the 4 types of LEDs, as illustrated in Figure 5c. To investigate if this order affects the IMD degradation efficiency at different wavelengths, the degradation was determined in the 4 microreactors at 395, 409, 413, and 443 nm applied in different order, by rotating the light source from position 1 to position 4. Figure 11 shows that the wavelength-dependent IMD degradation follows the same trend for all microreactors, which is 395 nm > 409 nm > 413nm > 443 nm. It was, therefore, demonstrated that it does not matter if the photocatalyst is tested first at 395 nm or 443 nm. What was found to matter is the time required for reaching the equilibrium state especially at the initial test, which could explain the lower degradation efficiency at 395 nm obtained in the microreactor M1. The larger values obtained in the microreactor M4 at all investigated wavelengths were attributed to a larger surface area of the photocatalyst which was in contact cu IMD solutions compared to the other microreactors.

To investigate if activity of the film suffers over time, the initial performed tests in each microreactor were repeated at the end of the multi-wavelength screening. Table 4 shows that the degradation efficiency increased in all cases after 6 h of operation compared to the values obtained after 2 h. This increase was observed also in our previous study and was attributed to the adsorption on the surface of products which improved the photocatalytic activity.[33] However, as this variation over time did not affect the relative activity at the 4 different illumination conditions, the results of such long-time tests can be used for identifying the suitable irradiation for the investigated photocatalysts.

Tabel 4 IMD degradation efficiency in the 4 microreactors at the same irradiating wavelength, λ_{max}, after 2 and 6 h of operation, representing the initial and final photocatalytic tests.

Microreactor	λ_{max}	IMD degradation efficiency (%)	
	(nm)	2 h operation	6 h operation
M1	395	27.9 ± 3.4	34.8 ± 2.6
M2	409	16.3 ± 2.0	21.4 ± 0.8
M3	443	1.0 ± 0.7	2.0 ± 0.6
M4	413	17.1 ± 0.8	18.1 ± 1.2

11

Noteworthy, each screening test in which 6 conditions were investigated, one in the dark and 5 under LEDs irradiation, consumed just 46 mg of photocatalyst and 21 mL of IMD solution.

3.2 Conditions optimization

At 395 nm, the IMD degradation efficiency obtained while characterizing the microfluidic platforms was around 35 %. Therefore, we looked into optimizing the reaction conditions to achieve a higher degree of IMD degradation and to accommodate the operation of 4 microreactors in parallel. Three types of conditions were tested: (i) dynamic flow and continuous irradiation, (ii) continuous flow and dynamic irradiation, and (iii) dynamic flow and dynamic irradiation. The tests were carried out on different photocatalytic films, after a preliminary test at 3.5 mL h^{-1} which was considered the reference IMD degradation. The reference test was performed for each photocatalytic film to take into consideration the variations caused by the material deposition and microreactor mounting.

As shown in Table 5, the highest degradation efficiency of around 71 % was achieved in the dynamic flow and continuous irradiation, when the liquid was periodically pumped at 7 mL h^{-1} for Time ON = 5 s and stopped for Time OFF = 19 s. This represents an increase by 1.8 times of the degradation efficiency obtained in the reference conditions and was attributed to increasing the residence time from 1.15 to 2.76 min. It is important to mention that the waiting time for reaching the steady state increased as well from 20 to 50 min. Then, by increasing Time ON to 10 and 15 s with the corresponding Time OFF of 34 and 49 s, the residence time decreases, and, therefore, the degradation efficiency drops to 59 and 50 %, respectively. Moreover, by increasing the infusion flow rate to 10.5 mL h^{-1}, the residence time becomes 1.6 min, and the degradation efficiency decreases to 38 %. It is, therefore, shown that the degradation efficiency can be controlled by varying the residence time using the periodic infusion-stop flow. However, as the increase was lower than expected, 1.8 vs. 2.4 times in the case of Time ON = 5 s, the observed degradation efficiency might be affected to a certain degree by mass transfer limitations.

Table 5 IMD degradation efficiency measured in microreactor M1 at various flow and illumination conditions. The reference IMD degradation efficiency is determined using the same immobilized TiO$_2$ P25 photocatalytic film at 3.5 mL h^{-1} before the corresponding photocatalytic test.

Flow rate	Dynamic flow configuration		Dynamic light configuration		Degradation efficiency	Reference Degradation efficiency
	Time ON	Time OFF	Time ON	Time OFF		
(mL h^{-1})	(s)	(s)	(s)	(s)	(%)	(%)
7	5	19	continuous	-	71.4 ± 2.2	39.2 ± 0.5
7	10	34	continuous	-	58.7 ± 2.4	31.0 ± 3.4
7	15	49	continuous	-	50.1 ± 1.4	33.3 ± 2.3
10.5	15	49	continuous	-	38.2 ± 0.1	36.4 ± 1.6
3.5	continuous	-	1	3	15.7 ± 0.3	30.2 ± 2.4
7	10	34	1	3	30.4 ± 0.9	29.1 ± 6.0
7	10	34	0.5	1.5	39.3 ± 0.9	42.3 ± 0.2

12

The dynamic illumination was implemented to power the 4 LEDs groups during a parallel screening experiment using a single power supply. At the continuous flow of 3.5 mL h^{-1} and dynamic irradiation characterized by Time ON = 1 s and Time OFF = 3 s, the IMD degradation efficiency halved to 15.7 % even though the 395 nm LEDs group emitted for just a quarter of the time compared to the case of the reference photocatalytic test. When the dynamic flow was combined with the dynamic irradiation, the resulted degradation efficiency was almost maintained compared to the reference test, because the improvement gained by the periodic infusion-stop flow was canceled by the periodic illumination at both 0.5 and 1 s. Nevertheless, the identified conditions permit keeping the same degradation efficiency at a lower energy consumption and simultaneous operation of the 4 microreactors.

4 Conclusions

In this study, the design, characterization and optimization of a new microfluidic platform for screening the photocatalytic activity of immobilized photocatalysts is presented. The developed screening platform is compact, modular and consists of four 3D printed microreactors illuminated by a multi-wavelength LED light source. The rotation of the light source emitting at 395, 409, 413 and 443 nm enables at least 16 photocatalytic tests in the 4 microreactors. The photoreactor system assembly was validated through the photocatalytic degradation of a pesticide, IMD, over immobilized films of TiO$_2$ P25. It was shown that for obtaining a reproducible and dependable testing of the photocatalytic activity of multiple photocatalytic films, a good control of the photocatalytic film thickness and photocatalyst surface area exposed to the IMD solution is required. Moreover, it was demonstrated that the screening order at 395, 409, 413, and 443 nm on the imidacloprid degradation by TiO2 P25 does not have an influence on the observed degradation efficiencies.

The optimization of the reaction conditions implied implementing dynamic flow and dynamic illumination which varied the residence times between 1.15 and 2.76 min, photon irradiances between 0.7 and 2.7·10^{-3} Einstein m^{-2} s^{-1}, and led to IMD degradation efficiencies between 15.7 and 71.4 %. The dynamic flow allowed increasing the degradation efficiency by a periodic infusion-stop flow which led to a longer residence time of the IMD solution in the microreactor. On the other hand, the dynamic illumination implied the sequential operation of the 4 types of LEDs, and led to a halved degradation efficiency despite applying a duty cycle of 25 %. The optimized conditions will allow future parallel screening in the 4 microreactors.

The developed microfluidic platform AutoMATiO represents a fast, cost-efficient and sustainable screening solution as it is manufactured mainly by 3D printed technique using biodegradable materials such as PLA and PHA and consumes a small amount of polluted water (21 mL) and photocatalytic material (46 mg) during 6 h operation at 6 screening conditions (1 in the dark and 5 under LEDs irradiation). We believe that this study will contribute to advancing the screening methods applied to immobilized photocatalysts and pave the way for more studies that focus on the wavelength-dependent photocatalytic activity.

This screening platform can be developed further for automated parallel testing by introducing distribution valves at the microreactors inlets and outlets and an in-line analysis instrument.

Acknowledgments

References

1   A. C. Sun, D. J. Steyer, A. R. Allen, E. M. Payne, R. T. Kennedy and C. R. J. Stephenson, *Nat. Commun.*, 2020, **11**, 6202.

2   A. C. Sun, D. J. Steyer, R. I. Robinson, C. Ginsburg-Moraff, S. Plummer, J. Gao, J. W. Tucker, D. Alpers, C. R. J. Stephenson and R. T. Kennedy, *Angewandte Chemie International Edition*, 2023, **62**, e202301664.

3   N. S. Eyke, T. N. Schneider, B. Jin, T. Hart, S. Monfette, J. M. Hawkins, P. D. Morse, R. M. Howard, D. M. Pfisterer, K. Y. Nandiwale and K. F. Jensen, *Chem Sci*, 2023, **14**, 8798–8809.

4   A. Slattery, Z. Wen, P. Tenblad, J. Sanjosé-Orduna, D. Pintossi, T. den Hartog and T. Noël, *Science (1979)*, 2024, **383**, eadj1817.

5   C. W. Coley, M. Abolhasani, H. Lin and K. F. Jensen, *Angew. Chem. Int. Ed.*, 2017, **56**, 9847–9850.

6   R. Gérardy, A. M. K. Nambiar, T. Hart, P. T. Mahesh and K. F. Jensen, *Chemistry – A European Journal*, 2022, **28**, e202201385.

7   M. Rößler and M. A. Liauw, *Chem. Methods*, 2021, **1**, 261–270.

8   C. C. Aletsee, D. Hochfilzer, A. Kwiatkowski, M. Becerer, J. Kibsgaard, I. Chorkendorff, M. Tschurl and U. Heiz, *Review of Scientific Instruments*, 2023, **94**, 033909.

9   H. E. Bonfield, K. Mercer, A. Diaz-Rodriguez, G. C. Cook, B. McKay, P. Slade, G. M. Taylor, W. X. Ooi, J. D. Williams, J. P. M. Roberts, J. A. Murphy, L. Schmermund, W. Kroutil, T. Mielke, J. Cartwright, G. Grogan and L. J. Edwards, *ChemPhotoChem*, 2020, **4**, 45–51.

10 K. Y. Nandiwale, T. Hart, A. F. Zahrt, A. M. K. Nambiar, P. T. Mahesh, Y. Mo, M. J. Nieves-Remacha, M. D. Johnson, P. García-Losada, C. Mateos, J. A. Rincón and K. F. Jensen, *React Chem Eng*, 2022, **7**, 1315–1327.

11 S. Knoll, C. E. Jusner, P. Sagmeister, J. D. Williams, C. A. Hone, M. Horn and C. O. Kappe, *React Chem Eng*, 2022, **7**, 2375–2384.

12 J. J. Mousseau, M. A. Perry, M. W. Bundesmann, G. M. Chinigo, C. Choi, G. Gallego, R. W. Hicklin, S. Hoy, D. C. Limburg, N. W. Sach and Y. Zhang, *ACS Catal*, 2022, **12**, 600–606.

13 K. Poscharny, D. C. Fabry, S. Heddrich, E. Sugiono, M. A. Liauw and M. Rueping, *Tetrahedron*, 2018, **74**, 3171–3175.

14 T. Roider, N. Frommknecht, A. Höltzel and U. Tallarek, *React Chem Eng*, 2022, **7**, 2035–2044.

15 C. D. Sahm, G. M. Ucoski, S. Roy and E. Reisner, *ACS Catal*, 2021, **11**, 11266–11277.

16 J. Li, F. Zhao, W. Fan, M. Chen and X. Guo, *Chemical Engineering Journal*, 2022, **447**, 137546.

17 K. Muzyka, K. Karim, A. Guerreiro, A. Poma and S. Piletsky, *Nanoscale Res Lett*, 2014, **9**, 154.

18 J. H. A. Schuurmans, T. M. Masson, S. D. A. Zondag, S. Pilon, N. Bragato, M. Claros, T. den Hartog, F. Sastre, J. ,[2] van den Ham, P. Buskens, G. Fiorani and T. Noël, *ChemRxiv*, , DOI:10.26434/chemrxiv-2024-sz6ng.

19 T. B. Engelhardt, S. Schmitz-Stöwe, T. Schwarz and K. Stöwe, *Materials*, 2020, **13**, 1365.

20   Y. Bi and P. Westerhoff, *Chemosphere*, 2019, **223**, 275–284.

21   J. Romão, D. Barata, P. Habibovic, G. Mul and J. Baltrusaitis, *Anal Chem*, 2014, **86**, 7612–7617.

22   J. Romão, D. Barata, N. Ribeiro, P. Habibovic, H. Fernandes and G. Mul, *Environmental Pollution*, 2017, **220**, 1199–1207.

23   N. M. Nursam, X. Wang and R. A. Caruso, *J Mater Chem A Mater*, 2015, **3**, 24557–24567.

24   K. Yanagiyama, K. Takimoto, S. Dinh Le, N. Nu Thanh Ton and T. Taniike, *Environmental Pollution*, 2024, **342**, 122974.

25   C. Lettmann, H. Hinrichs and W. F. Maier, *Angewandte Chemie International Edition*, 2001, **40**, 3160–3164.

26   Y. Li, B. Lin, L. Ge, H. Guo, X. Chen and M. Lu, *Sci. Rep.*, 2016, **6**, 28803.

27   H. Zhang, J.-J. Wang, J. Fan and Q. Fang, *Talanta*, 2013, **116**, 946–950.

28   T. B. Engelhardt, S. Schmitz-Stöwe, T. Schwarz and K. Stöwe, *ChemistryOpen*, 2022, **11**, e202200180.

29   T. B. Engelhardt, M. Zhu, C. Heilmann, S. Schmitz-Stöwe, T. Schwarz and K. Stöwe, *Catalysts*, , DOI:10.3390/catal11111351.

30   T. M. Kohl, Y. Zuo, B. W. Muir, C. H. Hornung, A. Polyzos, Y. Zhu, X. Wang and D. L. J. Alexander, *React Chem Eng*, 2024, **9**, 872–882.

31   R. Zhou, R. Han, M. Bingham, C. O'Rourke and A. Mills, *Photochem Photobiol Sci.*, 2022, **21**, 1585–1600.

32   Y. Sang, H. Liu and A. Umar, *ChemCatChem*, 2015, **7**, 559–573.

33   A. Roibu, R. Udroiu, C. Abreu-Jaureguí, J. Silvestre-Albero and L. Andronic, *J Environ Chem Eng*, 2024, **12**, 112752.

34   R. Udroiu, I. C. Braga and A. Nedelcu, *Materials*, , DOI:10.3390/ma12060995.

35   F. Xue, H. Deng, C. Xue, D. K. B. Mohamed, K. Y. Tang and J. Wu, *Chem Sci*, 2017, **8**, 3623–3627.

36   Q. Wang, R. Yin, Z. Wang, Y. Zhang and J. Wu, *J Flow Chem*, 2024, **14**, 97–107.

37   G.-N. Ahn, B. M. Sharma, S. Lahore, S.-J. Yim, S. Vidyacharan and D.-P. Kim, *Commun Chem*, 2021, **4**, 53.

38   S. Chatterjee, M. Guidi, P. H. Seeberger and K. Gilmore, *Nature*, 2020, **579**, 379–384.

39   C. Avila, C. Cassani, T. Kogej, J. Mazuela, S. Sarda, A. D. Clayton, M. Kossenjans, C. P. Green and R. A. Bourne, *Chem Sci*, 2022, **13**, 12087–12099.

40   M. Abolhasani and K. F. Jensen, *Lab Chip*, 2016, **16**, 2775–2784.

41   W. Debrouwer, W. Kimpe, R. Dangreau, K. Huvaere, H. P. L. Gemoets, M. Mottaghi, S. Kuhn and K. Van Aken, *Org Process Res Dev*, 2020, **24**, 2319–2325.

42   O. Tokode, R. Prabhu, L. A. Lawton and P. K. J. Robertson, *Chemical Engineering Journal*, 2014, **246**, 337–342.

43   Y. Ku, S.-J. Shiu and H.-C. Wu, *J Photochem Photobiol A Chem*, 2017, **332**, 299–305.

44   H.-W. Chen, Y. Ku and A. Irawan, *Chemosphere*, 2007, **69**, 184–190.

45   M. Vezzoli, T. Farrell, A. Baker, S. Psaltis, W. N. Martens and J. M. Bell, *Chem. Eng. J.*, 2013, **234**, 57–65.

46   D. Chen, F. Li and A. K. Ray, *Catal. Today*, 2001, **66**, 475–485.